A Novel Earthquake Early Warning System For the Marmara Region of Türkiye

Geo-INQUIRE installation: INFO – Irpinia Near Fault Observatory
Project title: A Novel Earthquake Early Warning System For the Marmara Region of Türkiye
Transnational access principal investigator: Ali Özgün Konca
Project acronym: NEWMAR
Project report ID: C3_TA3-84-1_3
Transnational access team: Ali Özgün Konca, Semih Ergintav, Fatih Turhan
Date of visit: from 13/05/2026 to 23/05/2026
Geo-INQUIRE Virtual Access: https://zenodo.org/records/21393935
Where are the results/data stored: Data available on the CREW Epos platform (**https://lccepos.fisica.unina.it/index.php?page=playbacks_geo-inquire_c3-ta3-84-1-3_quakeup_marmara.php**)

1. Introduction

As demonstrated by the devastating 2023 earthquake doublet in eastern Türkiye (Karabulut et al., 2023), earthquakes remain a major natural hazard that requires a wide range of mitigation strategies. A critical component of earthquake risk reduction is the establishment of reliable Earthquake Early Warning Systems (EEWS) (Rea et al., 2024). Within this framework, the Early Warning Team at Boğaziçi University's Kandilli Observatory and Earthquake Research Institute (KOERI) aims to develop a robust EEWS by integrating multiple early warning approaches. The long-term objective is to establish a comprehensive system that will initially serve the Marmara Supersite and subsequently expand to cover the entirety of Türkiye.

In this context, this study aims to optimize the recently developed QuakeUp EEWS using seismic recordings from stations distributed around the Sea of Marmara, which hosts the unruptured segment of the North Anatolian Fault Zone (NAFZ). QuakeUp (Zollo et al., 2023) is an EEWS that relies on rapid P-phase arrival determination to make an initial estimate of the earthquake location. The system relates the peak displacement (Pd), velocity (Pv), and acceleration (Pa) values measured on the vertical component to estimate the event magnitude from strong-motion data. Additionally, Peak Ground Velocity (PGV) is estimated by using both the vertical peak values measured within progressive time windows and Ground Motion Prediction Equations (GMPEs). Predicting the eventual peak ground motion and intensity metrics from these very short early P-wave windows requires the development and calibration of empirical relationships using regional seismic data from the Marmara region.

2. Dataset

2.1 Network and Event Selection

This report presents calibration of the QuakeUp Earthquake Early Warning (EEW) algorithm for the Marmara region of Türkiye. Regional empirical relationships were derived between early P-wave amplitude parameters, peak ground acceleration (Pa), velocity (Pv), and displacement (Pd), and both moment magnitude (Mw) and peak ground velocity (PGV).

In the first half of 2024, 20 low-latency accelerometers were added to the KOERI Marmara network, modifying the operational station configuration used by QuakeUp in the region (Figure 1). For this reason, events recorded after this network upgrade were preferentially selected for calibration, so that the empirical relationships would reflect the current operational

network geometry and station availability. Reference Mw values were obtained from the KOERI catalog, where Mw is estimated through S-wave displacement spectral fitting.

QuakeUp records peak ground velocity on all three components in its log files. Since Akkar and Bommer (2007) derive their GMPE for the geometric mean of the two horizontal components, we computed PGV_GM from the QuakeUp logs and used this as the calibration target.

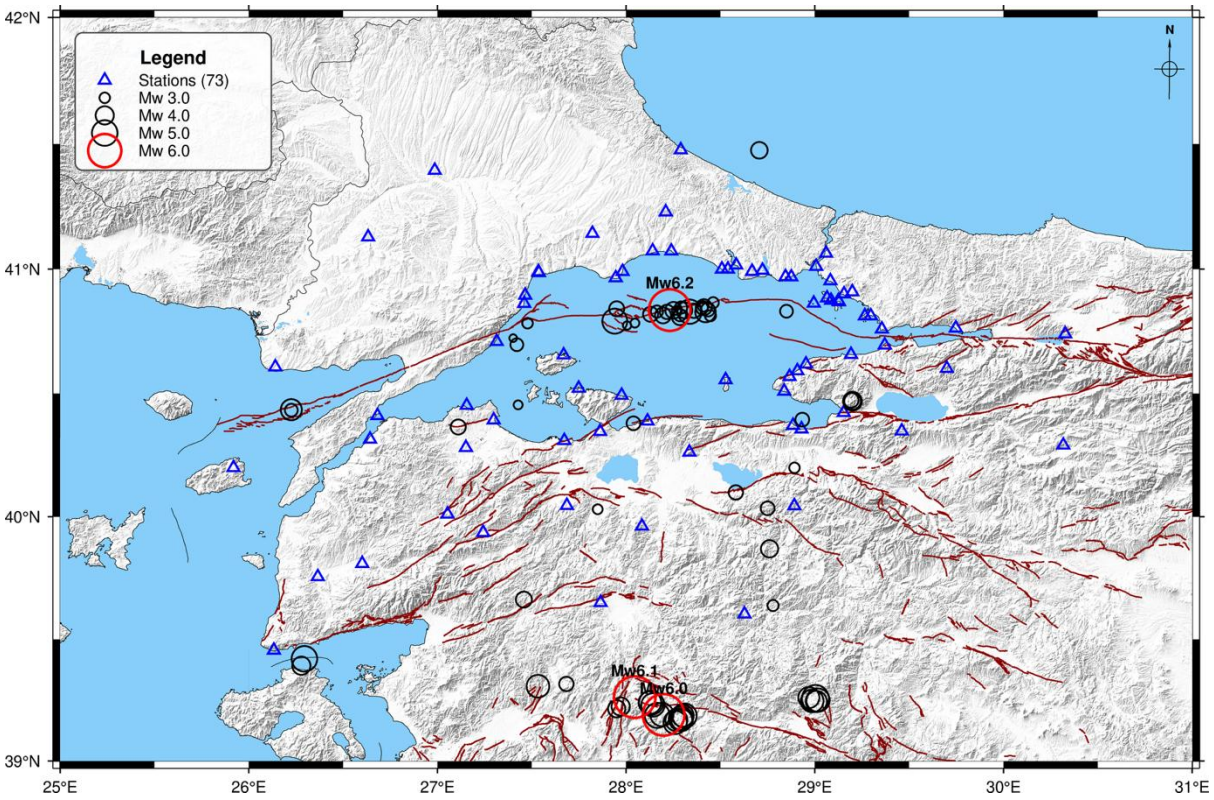

Figure 1. Map of the 70 calibration events and stations used in this study. Earthquakes are represented by circles, with symbol size proportional to Mw; events with Mw ≥ 6.0 are highlighted in red. Stations are represented by open blue triangles.

Candidate events were selected from the KOERI earthquake catalog and processed with QuakeUp in playback mode to generate the calibration dataset. The final dataset consists of 70 earthquakes recorded between June 2024 and February 2026, covering a magnitude range from Mw 2.7 to Mw 6.2. Events were selected based on two main criteria: (1) a minimum of 15 station recordings per event, and (2) geographic filtering to prioritize earthquakes located within or near the Marmara network footprint. QuakeUp-derived peak displacement (Pd), velocity (Pv), and acceleration (Pa) measurements were extracted from eight cumulative P-wave time windows selected to sample both the rapid early evolution and the later stabilization of the P-wave peak parameters. The resulting dataset contains 84,065 station-window records spanning hypocentral distances from approximately 5 to 235 km. Figure 2 shows the magnitude–distance distribution of the seismic records used for calibration, while the complete event list is provided in Appendix A.

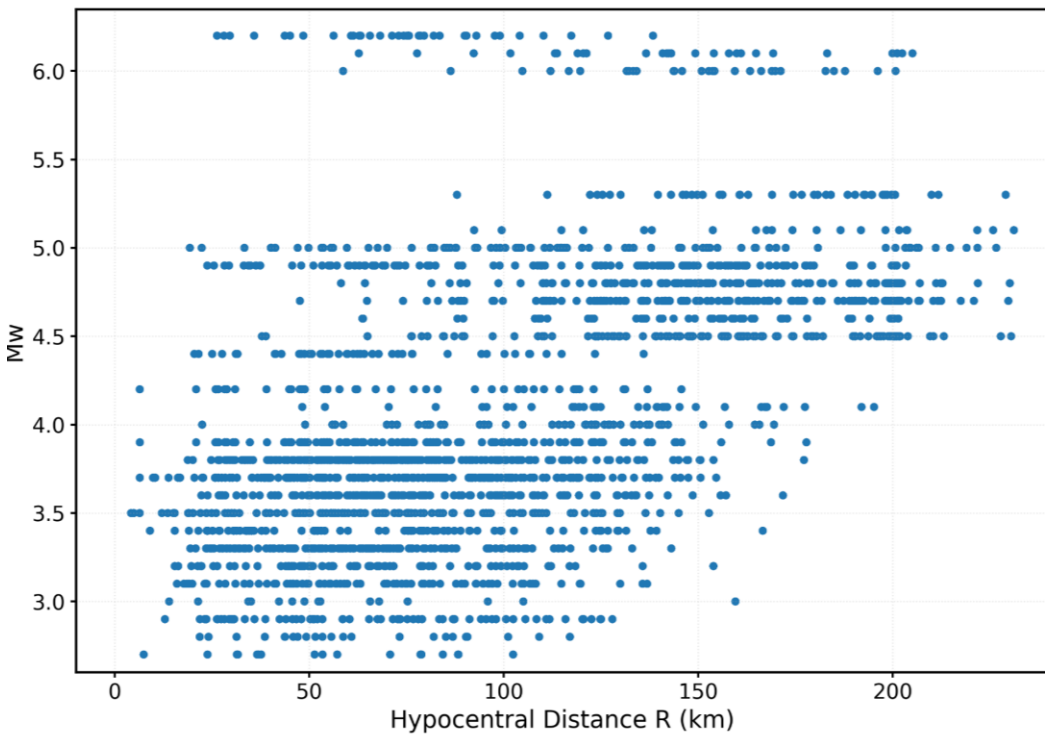

Figure 2. Station records in Mw–distance space (Win < 20 s, 70 events).

3. Calibration Methodology

3.1 Empirical Formulas

QuakeUp utilizes a linear relationship between the logarithm of measured peak values from vertical recordings, logarithm of distance and magnitude:

$$\mathbf{Mw = A + B \cdot \log_{10}(Px) + C \cdot \log_{10}(R)}$$

Since the estimated horizontal PGV is an on site estimate from the vertical recording, the equation only involves the peak values:

$$\mathbf{\log_{10}(PGV_GM) = A + B \cdot \log_{10}(Px)}$$

where Px ∈ {Pa, Pv, Pd} and R is hypocentral distance in km. The estimate of Mw and PGV is calculated from estimate from each Px weighted by sigma (σ_x), where σ_x is the standard deviation obtained from optimization from the regression.

3.2 Regression Method and Data Balancing

Our approach for optimizing the parameters for Mw estimation is based on 2D median binning of the available measurements in the Mw–log(distance) space. For PGV estimation, 1D median binning is applied along $\log_{10}$(Px). For the regression we utilize Orthogonal Distance Regression - ODR (Boggs & Rogers 1990; scipy.odr) which minimizes residuals orthogonally in both axes.

Our initial attempt to fit all available data was not satisfactory since when we use all available data, outliers and anomalous values have too significant an effect and also since the catalog is dominated by small earthquakes. To address this imbalance, 2D median binning was applied: the (Mw, $\log_{10}$R) space was divided into 0.1×0.1 cells; the median of Px, Mw, and $\log_{10}$R within each occupied cell was computed; and ODR was fitted to the resulting median points with equal weights. For PGV, 1D binning along $\log_{10}$(Px) was applied (bin width = 0.05 log units).

3.3 Time Window Structure

Because the Mw and PGV estimates depend on the length of the time window measured from the first P-wave arrival, the parameter optimization was performed separately for a range of time-window lengths. These windows were selected to sample the rapid early evolution of the P-wave peak parameters while also capturing their later stabilization. The number of available records for each time window is summarized in Table 1.

Calibration bin	win_Pz values included	Records
Win < 1.1 s	0.5, 1.0 s	4,204
Win < 2.1 s	1.5, 2.0 s	4,204
Win < 3.1 s	2.5, 3.0 s	4,204
Win < 4.6 s	3.5, 4.0, 4.5 s	6,306
Win < 6.6 s	5.0–6.5 s (4 steps)	8,408
Win < 8.6 s	7.0–8.5 s (4 steps)	8,408
Win < 12.1 s	9.0–12.0 s (7 steps)	14,712
Win < 20 s	12.5–20.0 s (16 steps)	33,619

Table 1. Calibration bins, constituent win_Pz values, and record counts (70 events).

4. Calibration Results

Figure 3 compares the calibrated Mw estimates derived from Pa, Pv, and Pd with the corresponding catalog Mw values. The median values exhibit a clear linear relationship, indicating that the parameter optimization procedure successfully captures the dependence between the observed parameters and earthquake magnitude. Tables 2, 3, and 4 summarize the optimized coefficients obtained for each regression model.

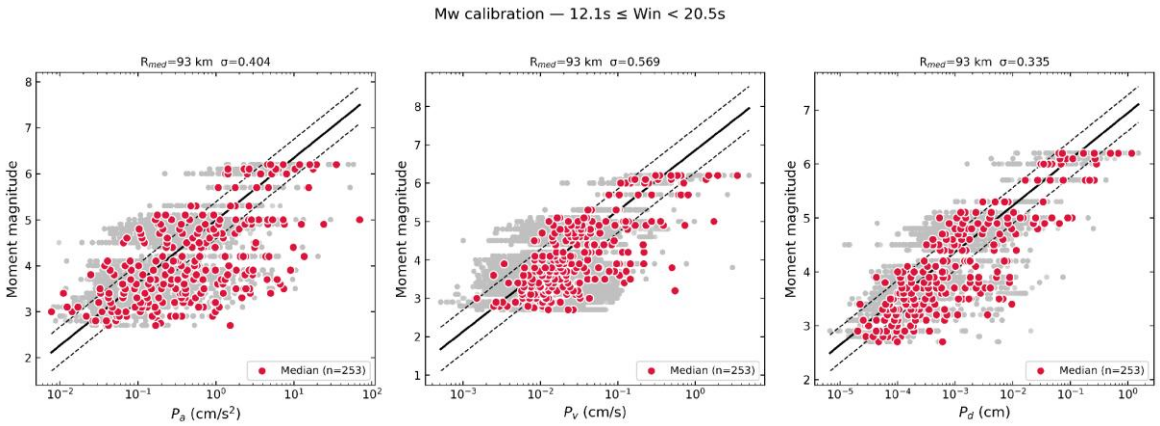

Figure 3. Calibrated Mw scaling relationships derived from Pa, Pv, and Pd for the 12.1–20s time window. Gray symbols show individual station measurements, red symbols represent median-binned observations used in the regression, the solid line indicates the fitted model, and dashed lines denote ±σ. All other calibration windows are provided in Appendix B.

Window	A (±sd)	B (±sd)	C (±sd)	σ
< 1.1s	-2.7326 (0.3576)	2.0403 (0.1051)	4.7209 (0.2343)	0.908
< 2.1s	-0.8594 (0.1749)	1.6062 (0.0494)	3.2702 (0.1063)	0.587
< 3.1s	-0.3828 (0.1411)	1.4928 (0.0389)	2.9071 (0.0839)	0.509
< 4.6s	-0.2184 (0.1265)	1.4438 (0.0343)	2.7683 (0.0745)	0.464
< 6.6s	-0.1114 (0.1184)	1.4079 (0.0316)	2.6728 (0.0692)	0.434
< 8.6s	-0.1178 (0.1180)	1.4008 (0.0313)	2.6607 (0.0687)	0.415
< 12.1s	-0.1020 (0.1174)	1.3882 (0.0309)	2.6323 (0.0681)	0.408
< 20s	0.0300 (0.1164)	1.3607 (0.0304)	2.5166 (0.0669)	0.404

Table 2. Optimized Mw calibration coefficients derived from Pa for all time windows. Coefficients correspond to the relationship $Mw = A + B \log_{10}(Pa) + C \log_{10}(R)$. The reported σ values represent the standard deviation of Mw residuals.

Window	A (±sd)	B (±sd)	C (±sd)	σ
< 1.1s	2.4917 (0.2291)	1.9826 (0.0949)	3.1642 (0.1617)	0.814
< 2.1s	2.8540 (0.1705)	1.7213 (0.0621)	2.5369 (0.1085)	0.631
< 3.1s	2.9014 (0.1487)	1.6305 (0.0516)	2.3447 (0.0922)	0.576
< 4.6s	2.9497 (0.1369)	1.6009 (0.0468)	2.2331 (0.0836)	0.552
< 6.6s	2.9144 (0.1366)	1.5790 (0.0461)	2.1753 (0.0827)	0.544
< 8.6s	2.8933 (0.1366)	1.5749 (0.0460)	2.1426 (0.0823)	0.544
< 12.1s	2.8771 (0.1384)	1.5721 (0.0465)	2.1027 (0.0829)	0.549

Window	A (±sd)	B (±sd)	C (±sd)	σ
< 20s	2.9580 (0.1400)	1.5729 (0.0470)	1.9773 (0.0821)	0.569

Table 3. Optimized Mw calibration coefficients derived from Pv for all time windows. Coefficients correspond to the relationship Mw = A + B $\log_{10}$(Pv) + C $\log_{10}$(R). The reported σ values represent the standard deviation of Mw residuals.

Window	A (±sd)	B (±sd)	C (±sd)	σ
< 1.1s	4.2826 (0.1784)	1.2780 (0.0442)	2.4945 (0.1034)	0.584
< 2.1s	4.2152 (0.1349)	1.0383 (0.0277)	1.9303 (0.0730)	0.442
< 3.1s	4.2023 (0.1165)	0.9894 (0.0230)	1.7964 (0.0625)	0.400
< 4.6s	4.2999 (0.0987)	0.9600 (0.0190)	1.6477 (0.0521)	0.369
< 6.6s	4.2799 (0.0880)	0.9241 (0.0164)	1.5546 (0.0463)	0.352
< 8.6s	4.2192 (0.0824)	0.8838 (0.0148)	1.4876 (0.0434)	0.329
< 12.1s	4.1881 (0.0807)	0.8740 (0.0144)	1.4645 (0.0425)	0.327
< 20s	4.2384 (0.0774)	0.8603 (0.0136)	1.3760 (0.0404)	0.335

Table 4. Optimized Mw calibration coefficients derived from Pd for all time windows. Coefficients correspond to the relationship Mw = A + B $\log_{10}$(Pd) + C $\log_{10}$(R). The reported σ values represent the standard deviation of Mw residuals.

Figure 4 shows the calibrated PGV scaling relationships derived from Pa, Pv, and Pd. The fitted models reproduce the median-binned observations well. Tables 5, 6, and 7 summarize the optimized coefficients obtained for the PGV regression models.

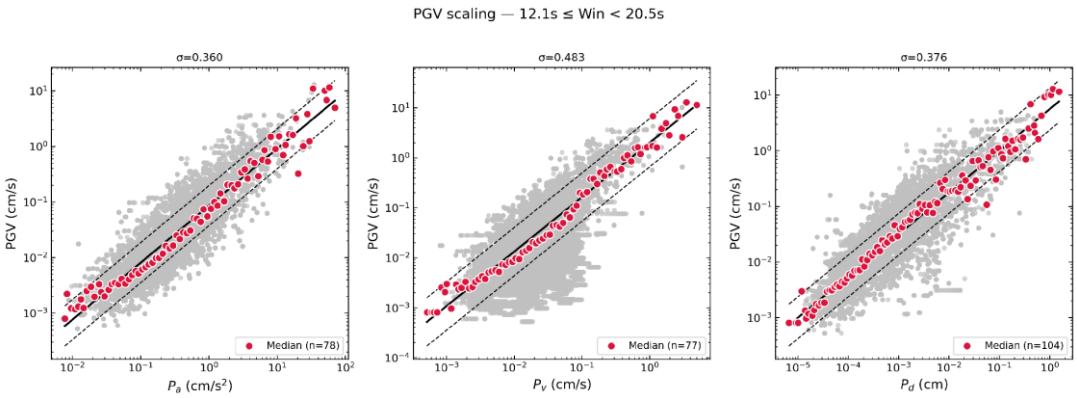

Figure 4. Calibrated PGV scaling relationships derived from Pa, Pv, and Pd for the 12.1–20s time window. Gray symbols show individual station measurements, red symbols represent median-binned observations used in the regression, the solid line indicates the fitted model, and dashed lines denote ±σ. All other calibration windows are provided in Appendix C.

Window	A (±sd)	B (±sd)	σ
< 1.1s	-0.9037 (0.0366)	0.8050 (0.0291)	0.623
< 2.1s	-0.9302 (0.0272)	0.9411 (0.0231)	0.483
< 3.1s	-0.9398 (0.0266)	1.0011 (0.0230)	0.423
< 4.6s	-0.9602 (0.0248)	1.0151 (0.0215)	0.397
< 6.6s	-0.9734 (0.0258)	1.0258 (0.0224)	0.385
< 8.6s	-1.0122 (0.0240)	1.0246 (0.0213)	0.381
< 12.1s	-1.0361 (0.0236)	1.0245 (0.0206)	0.380
< 20s	-1.0717 (0.0232)	1.0254 (0.0202)	0.360

Table 5. Optimized PGV calibration coefficients derived from Pa for all time windows. Coefficients correspond to the relationship $\log_{10}(PGV) = A + B \log_{10}(Pa)$. The reported σ values represent the standard deviation of residuals in $\log_{10}(PGV)$ space.

Window	A (±sd)	B (±sd)	σ
< 1.1s	0.6127 (0.0823)	0.9946 (0.0392)	0.603
< 2.1s	0.6337 (0.0638)	1.0557 (0.0316)	0.503
< 3.1s	0.5800 (0.0578)	1.0613 (0.0300)	0.469
< 4.6s	0.4769 (0.0581)	1.0401 (0.0302)	0.464
< 6.6s	0.4733 (0.0557)	1.0553 (0.0287)	0.468
< 8.6s	0.4168 (0.0540)	1.0418 (0.0285)	0.476
< 12.1s	0.3390 (0.0412)	1.0387 (0.0223)	0.481
< 20s	0.2981 (0.0314)	1.0897 (0.0178)	0.483

Table 6. Optimized PGV calibration coefficients derived from Pv for all time windows. Coefficients correspond to the relationship $\log_{10}(PGV) = A + B \log_{10}(Pv)$. The reported σ values represent the standard deviation of residuals in $\log_{10}(PGV)$ space.

Window	A (±sd)	B (±sd)	σ
< 1.1s	1.2815 (0.0453)	0.7717 (0.0134)	0.512
< 2.1s	1.2021 (0.0529)	0.7839 (0.0164)	0.422
< 3.1s	1.1572 (0.0491)	0.7889 (0.0156)	0.392
< 4.6s	1.1633 (0.0372)	0.8031 (0.0122)	0.393
< 6.6s	0.9804 (0.0361)	0.7654 (0.0117)	0.399
< 8.6s	0.8482 (0.0362)	0.7403 (0.0119)	0.396

Window	A (±sd)	B (±sd)	σ
< 12.1s	0.7888 (0.0311)	0.7376 (0.0104)	0.390
< 20s	0.7450 (0.0335)	0.7500 (0.0115)	0.376

Table 7. Optimized PGV calibration coefficients derived from Pd for all time windows. Coefficients correspond to the relationship $log_{10}(PGV) = A + B\ log_{10}(Pd)$. The reported σ values represent the standard deviation of residuals in $log_{10}(PGV)$ space.

The optimized calibration parameters were further evaluated using QuakeUp playbacks of representative Marmara earthquakes, including events both within and outside the calibration dataset. Playback results for 10 representative earthquakes are provided in Appendix D.

As a representative case example, Figure 5 shows the QuakeUp playback result for the 23 April 2025 Mw 6.2 Marmara Sea earthquake. The optimized calibration accurately estimates the event magnitude as Mw 6.2. Previous studies indicate that this earthquake ruptured unilaterally toward the east (Martínez-Garzón et al., 2025). Consistent with this rupture directivity, the QuakeUp shake-map estimate is asymmetric around the epicenter, with higher intensity values east of Istanbul than at comparable distances to the west. This pattern suggests that the optimized QuakeUp shake map captures the influence of finite-fault directivity on the predicted intensity distribution.

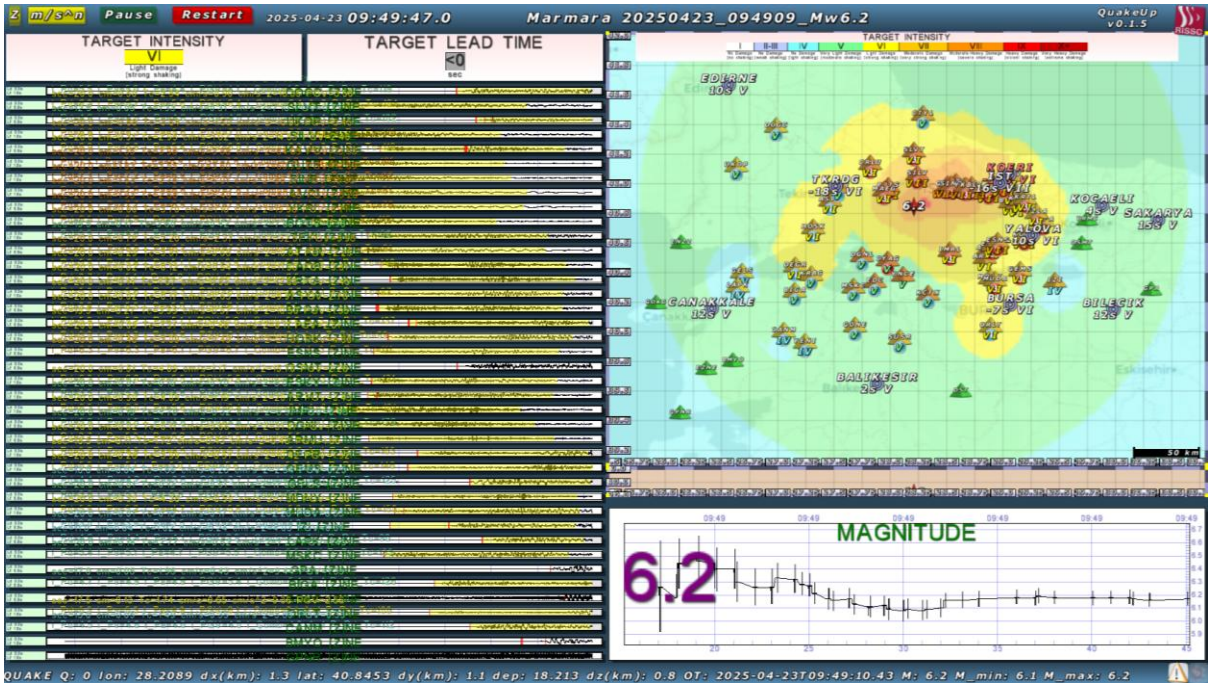

Figure 5. Simulation results and the QuakeUp shake map for the 23 April 2025 Mw 6.2 Marmara Sea earthquake. The left panel shows the waveform recordings, the upper-right panel shows the estimated intensity map, and the lower-right panel shows the estimated magnitude as a function of time.

5. Conclusion

In this Transnational Access study, with the support of experts from the Irpinia Near-Fault Observatory, we developed a workflow that successfully estimates PGV and intensity and produces an early warning (EEW) alert within several seconds after P-wave onset, using a minimum number of stations. For the Marmara region, this threshold is four stations.

Our objective is to implement QuakeUp together with the Virtual Seismologist (Cua, 2005; Cua and Heaton, 2007; Cua et al., 2009) and to generate rapid shake maps for both the Kandilli Observatory and Earthquake Research Institute website and our in-house iOS-based EEW mobile application.

References

Akkar, S. and Bommer, J.J. (2007). Empirical prediction equations for peak ground velocity derived from strong-motion records from Europe and the Middle East. Bulletin of the Seismological Society of America, 97(2), 511–530.

Boggs, P.T. and Rogers, J.E. (1990). Orthogonal distance regression. Contemporary Mathematics, 112, 183–194.

Caruso, A. (2018). Calibration of QuakeUp EEW algorithms. RISSC-Lab Internal Report, University of Naples Federico II.

Cua, G. (2005). Creating the Virtual Seismologist: Developments in ground motion characterization and seismic early warning (PhD thesis). California Institute of Technology, Pasadena, CA.

Cua, G., & Heaton, T. (2007). The Virtual Seismologist (VS) method: A Bayesian approach to earthquake early warning. In P. Gasparini, G. Manfredi, & J. Zschau (Eds.), Seismic Early Warning (pp. 85–132). Springer.

Cua, G., Fischer, M., Heaton, T., & Wiemer, S. (2009). Real-time performance of the Virtual Seismologist earthquake early warning algorithm in southern California. Seismological Research Letters, 80, 740–747.

Martínez-Garzón P. et al. 2025. Progressive eastward rupture of the main marmara fault toward Istanbul, Science. 391, 379–383.

Rea, R., Colombelli, S., Elia, L. et al. (2024). Retrospective performance analysis of a ground shaking early warning system for the 2023 Turkey–Syria earthquake. Communications Earth & Environment, 5, 332.

Zollo, A., Colombelli, S., Caruso, A., and Elia, L. (2023). An evolutionary shaking-forecast-based earthquake early warning method. Earth and Space Science, 10, e2022EA002657.

Appendix A: Calibration Event Catalog

The 70 earthquakes used for calibration are listed chronologically. Reference Mw values were obtained from the KOERI catalog, where Mw is estimated through S-wave displacement spectral fitting. All selected events have at least 15 station recordings.

#	Date	Time (UTC)	Lat (°N)	Lon (°E)	Depth (km)	Mw	Region
1	2024.06.13	08:27:13	40.3645	27.11	12.3	3.7	ESKIBALIKLI-BIGA (CANAKKALE)
2	2024.06.17	14:18:58	40.6968	27.4202	10.0	3.4	GUZELKOY ACIKLARI-TEKIRDAG (MARMARA DENIZI)
3	2024.06.24	22:36:44	39.3077	27.5322	5.3	4.7	VAKIFLI-SOMA (MANISA)
4	2024.07.18	17:29:19	40.199	28.8922	3.3	3.1	YAYLACIK-NILUFER (BURSA)
5	2024.08.03	02:05:34	39.8697	28.7602	6.3	4.0	GAZIOLUK-ORHANELI (BURSA)
6	2024.08.04	21:34:07	40.783	27.4777	9.1	3.1	YENIKOY ACIKLARI-TEKIRDAG (MARMARA DENIZI)
7	2024.08.15	03:20:30	40.3943	28.9335	12.1	3.5	MUDANYA (BURSA)
8	2024.09.04	08:38:15	40.723	27.4008	10.6	2.7	GUZELKOY ACIKLARI-TEKIRDAG (MARMARA DENIZI)
9	2024.09.24	01:20:21	39.663	27.4577	12.6	3.8	EVCILER-IVRINDI (BALIKESIR)
10	2024.10.27	14:56:00	39.3917	26.2788	7.9	4.1	MIDILLI ADASI (EGE DENIZI)
11	2024.12.12	11:34:52	40.4343	26.225	14.1	4.5	SAROS KORFEZI (EGE DENIZI)
12	2024.12.22	12:08:13	40.8407	27.9502	8.6	3.7	MARMARA EREGLISI ACIKLARI-TEKIRDAG (MARMARA DENIZI)
13	2025.01.10	09:24:55	40.813	28.4472	5.9	3.2	MARMARA DENIZI
14	2025.01.21	20:38:43	39.4205	26.2942	10.3	5.1	EDREMIT KORFEZI (EGE DENIZI)
15	2025.03.24	23:26:03	40.4538	27.4275	4.5	2.9	AVSA-MARMARA (BALIKESIR)
16	2025.04.07	17:39:59	40.099	28.581	8.4	3.6	DORAK-MUSTAFAKEMALPASA (BURSA)
17	2025.04.19	04:09:59	40.4323	26.225	15.3	3.4	SAROS KORFEZI (EGE DENIZI)
18	2025.04.22	20:24:50	40.3792	28.0383	5.8	3.5	DUTLIMAN-BANDIRMA (BALIKESIR)
19	2025.04.23	09:49:09	40.8355	28.2307	12.1	6.2	SILIVRI ACIKLARI-ISTANBUL (MARMARA DENIZI)
20	2025.04.23	12:12:57	40.8292	28.3365	11.4	4.9	MARMARA DENIZI
21	2025.04.23	14:43:31	40.8333	28.3597	11.5	3.6	MARMARA DENIZI
22	2025.04.23	14:47:55	40.8505	28.4077	19.2	3.1	MARMARA DENIZI
23	2025.04.23	16:12:24	40.8443	28.4012	7.7	3.3	MARMARA DENIZI
24	2025.04.23	18:46:28	40.8287	28.2163	14.4	3.6	SILIVRI ACIKLARI-ISTANBUL (MARMARA DENIZI)
25	2025.04.23	21:00:15	40.8353	28.3082	12.0	3.8	MARMARA DENIZI
26	2025.04.24	01:20:03	40.8192	28.1297	13.0	3.7	MARMARA DENIZI
27	2025.04.25	04:23:43	39.2612	28.9682	8.1	4.5	KARAKOCA-SIMAV (KUTAHYA)
28	2025.04.25	07:20:02	39.247	28.9858	6.1	4.7	YEMISLI-SIMAV (KUTAHYA)
29	2025.04.25	11:49:17	40.8653	28.461	19.8	3.2	GURPINAR ACIKLARI-ISTANBUL (MARMARA DENIZI)
30	2025.04.25	17:21:46	40.8373	28.4333	7.6	3.5	MARMARA DENIZI
31	2025.04.25	17:33:16	40.8278	28.4202	11.7	4.4	MARMARA DENIZI
32	2025.04.28	01:24:11	40.8458	28.2913	13.0	3.3	MARMARA DENIZI
33	2025.05.02	08:30:08	40.831	28.85	19.4	3.4	MARMARA DENIZI
34	2025.05.03	08:36:54	40.8145	28.1952	10.2	3.8	SILIVRI ACIKLARI-ISTANBUL (MARMARA DENIZI)

#	Date	Time (UTC)	Lat (°N)	Lon (°E)	Depth (km)	Mw	Region
35	2025.05.07	05:07:28	40.7837	28.046	12.4	2.9	MARMARA DENIZI
36	2025.05.09	23:28:08	40.8347	28.2663	15.0	2.9	SILIVRI ACIKLARI-ISTANBUL (MARMARA DENIZI)
37	2025.05.13	04:18:15	40.847	28.4118	10.6	3.8	MARMARA DENIZI
38	2025.05.13	17:46:31	40.835	28.2508	9.5	3.9	SILIVRI ACIKLARI-ISTANBUL (MARMARA DENIZI)
39	2025.06.01	07:15:32	40.031	27.8488	11.0	3.0	DARICA-MANYAS (BALIKESIR)
40	2025.07.01	08:47:20	40.4727	29.1922	9.3	3.7	SAHINYURDU-GEMLIK (BURSA)
41	2025.07.01	09:57:34	40.4687	29.2	9.6	3.9	SAHINYURDU-GEMLIK (BURSA)
42	2025.07.02	10:57:43	40.4688	29.1993	6.2	4.2	SAHINYURDU-GEMLIK (BURSA)
43	2025.07.05	11:24:21	40.8075	28.2848	13.7	3.8	SILIVRI ACIKLARI-ISTANBUL (MARMARA DENIZI)
44	2025.08.10	16:53:46	39.2632	28.0455	7.4	6.1	KIZILGUR-SINDIRGI (BALIKESIR)
45	2025.08.11	16:37:00	39.2245	27.9713	9.6	4.1	HACET-KIRKAGAC (MANISA)
46	2025.08.11	18:32:36	39.2148	27.9497	9.5	4.0	HACET-KIRKAGAC (MANISA)
47	2025.08.20	16:57:37	40.8152	28.2852	7.2	3.3	SILIVRI ACIKLARI-ISTANBUL (MARMARA DENIZI)
48	2025.09.05	00:10:08	40.83	28.1632	14.8	3.3	MARMARA DENIZI
49	2025.09.07	09:35:08	39.1913	28.1893	12.2	4.8	YAYLACIK-SINDIRGI (BALIKESIR)
50	2025.09.21	21:05:46	39.1882	28.165	9.6	5.0	SINANDEDE-SINDIRGI (BALIKESIR)
51	2025.09.28	09:59:15	39.2575	29.003	6.3	5.3	YESILDERE-SIMAV (KUTAHYA)
52	2025.09.28	22:48:28	39.2455	29.008	6.2	4.5	YEMISLI-SIMAV (KUTAHYA)
53	2025.10.02	11:55:03	40.7913	27.9395	7.7	5.0	MARMARA DENIZI
54	2025.10.04	19:06:04	39.6387	28.779	9.1	3.2	ADAOREN-DURSUNBEY (BALIKESIR)
55	2025.10.08	23:54:05	39.2507	29.0163	11.3	4.8	YESILDERE-SIMAV (KUTAHYA)
56	2025.10.26	16:44:50	41.4742	28.7057	15.1	3.9	ORMANLI ACIKLARI-ISTANBUL (KARADENIZ)
57	2025.10.27	19:48:28	39.19	28.1988	10.9	6.0	YAYLACIK-SINDIRGI (BALIKESIR)
58	2025.10.28	07:10:00	39.168	28.2667	11.8	4.6	ISIKLAR-SINDIRGI (BALIKESIR)
59	2025.10.28	07:54:12	39.1592	28.2598	7.7	4.8	BAYRAKLI-SINDIRGI (BALIKESIR)
60	2025.10.31	02:04:46	40.7737	28.0045	11.0	2.8	MARMARA DENIZI
61	2025.11.03	12:35:36	39.1868	28.3097	13.2	4.9	BUYUKDAGDERE-SINDIRGI (BALIKESIR)
62	2025.11.10	18:20:51	39.2407	28.126	13.3	4.7	BAYIRLI-SINDIRGI (BALIKESIR)
63	2025.11.10	02:49:11	39.231	28.1417	7.5	4.8	MANDIRA-SINDIRGI (BALIKESIR)
64	2025.11.13	03:16:14	39.2403	28.1323	10.3	4.9	MANDIRA-SINDIRGI (BALIKESIR)
65	2025.12.11	07:06:14	39.187	28.2993	13.6	4.6	BUYUKDAGDERE-SINDIRGI (BALIKESIR)
66	2026.01.14	23:03:10	39.3173	27.6832	12.3	3.6	GOKTAS-SOMA (MANISA)
67	2026.01.21	15:11:49	39.1698	28.2918	5.4	4.7	ISIKLAR-SINDIRGI (BALIKESIR)
68	2026.01.21	20:28:55	39.1698	28.2942	6.2	4.5	ISIKLAR-SINDIRGI (BALIKESIR)
69	2026.01.23	21:24:37	39.174	28.2902	12.0	4.9	ISIKLAR-SINDIRGI (BALIKESIR)
70	2026.02.14	11:34:52	40.0347	28.75	5.8	3.5	ESKIKIZILELMA-MUSTAFAKEMALPASA (BURSA)

Appendix B: Per-Window Scaling Figures — Mw

Three-panel figures showing Mw scaling relationships derived from Pa, Pv, and Pd for each calibration bin. Gray symbols show individual station measurements, red symbols represent 2D median-binned observations used in the regression, solid lines indicate the fitted models evaluated at the median hypocentral distance, and dashed lines denote ±σ in Mw units.

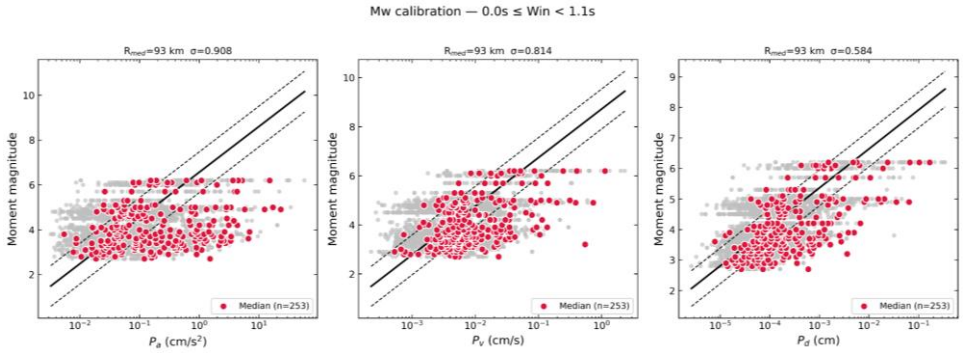

Mw scaling from Pa, Pv, and Pd — Win < 1.1 s

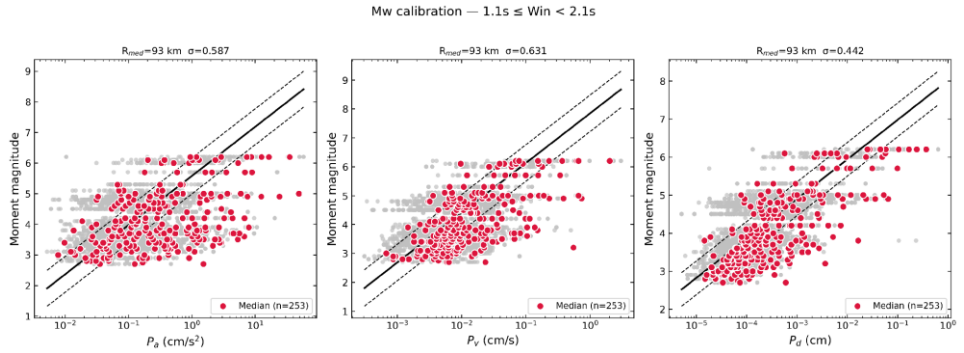

Mw scaling from Pa, Pv, and Pd — Win < 2.1 s

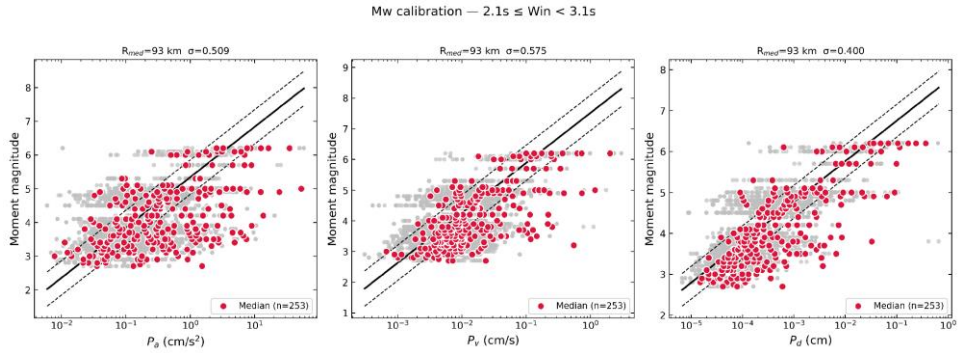

Mw scaling from Pa, Pv, and Pd — Win < 3.1 s

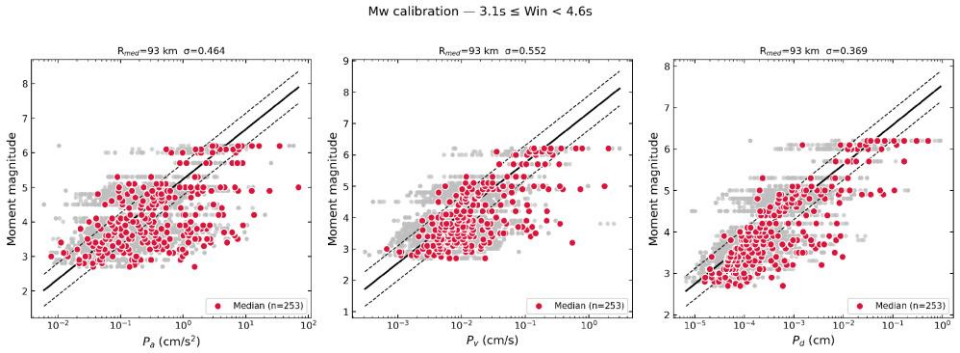

Mw scaling from Pa, Pv, and Pd — Win < 4.6 s

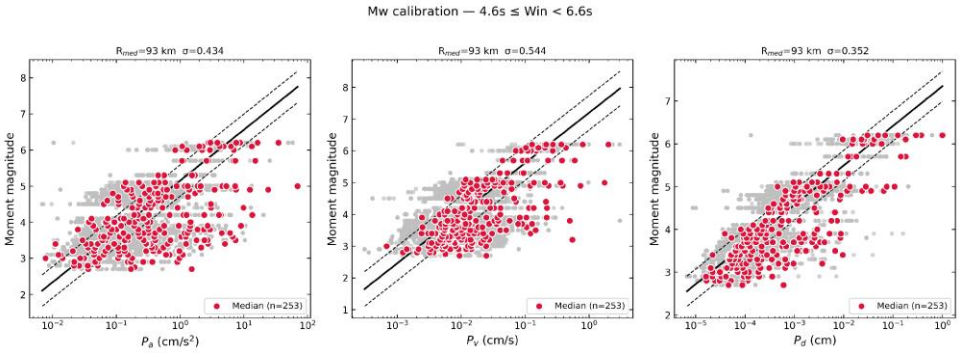

Mw scaling from Pa, Pv, and Pd — Win < 6.6 s

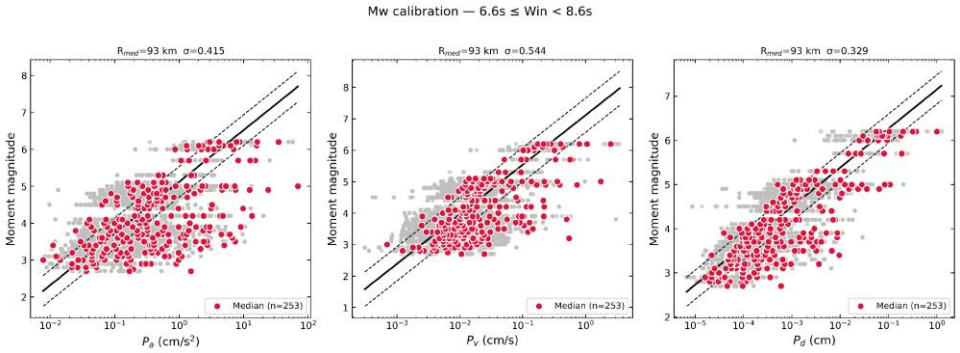

Mw scaling from Pa, Pv, and Pd — Win < 8.6 s

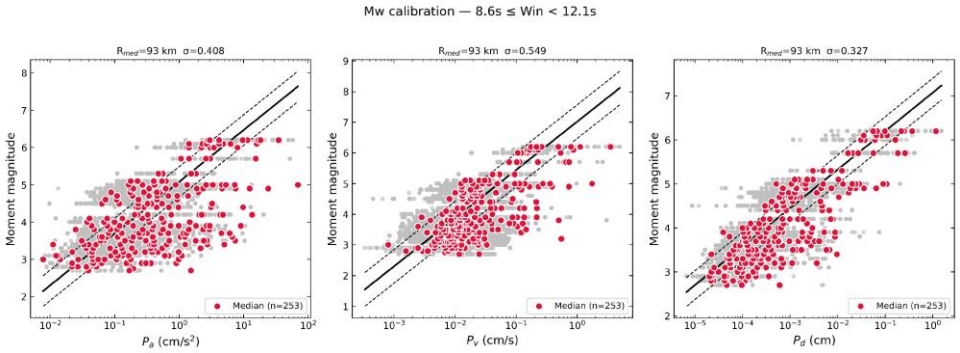

Mw scaling from Pa, Pv, and Pd — Win < 12.1 s

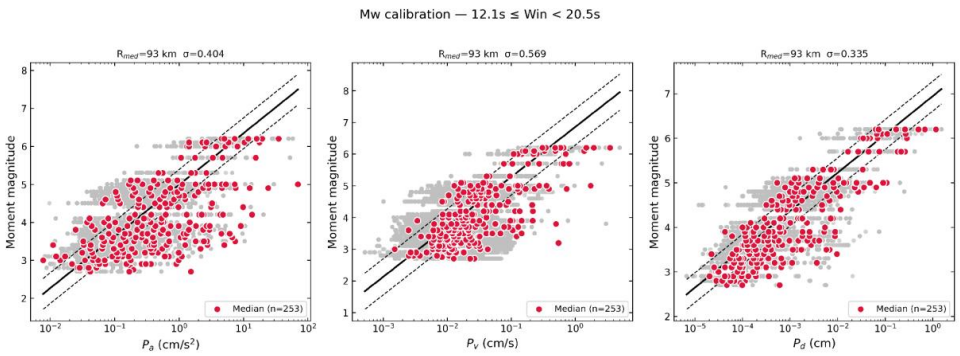

Mw scaling from Pa, Pv, and Pd — Win < 20 s

Appendix C: Per-Window Scaling Figures — PGV

Three-panel figures showing PGV_GM scaling relationships derived from Pa, Pv, and Pd for each calibration bin. Log–log axes are used in all panels. Gray symbols show individual station measurements, red symbols represent 1D median-binned observations used in the regression, solid lines indicate the fitted models, and dashed lines denote ±σ.

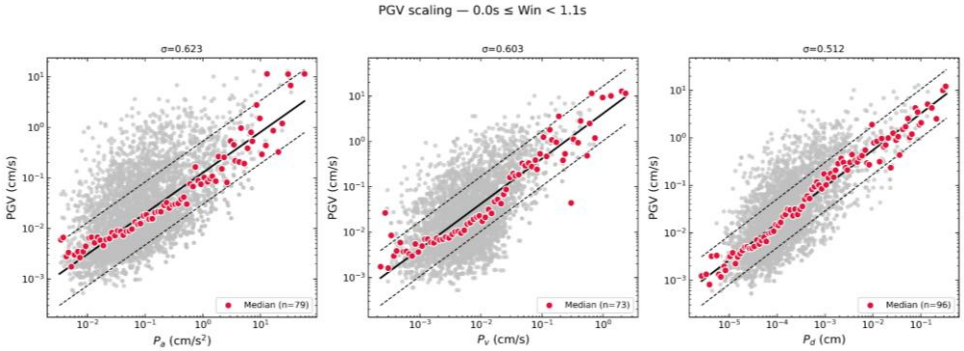

PGV scaling from Pa, Pv, and Pd — Win < 1.1 s

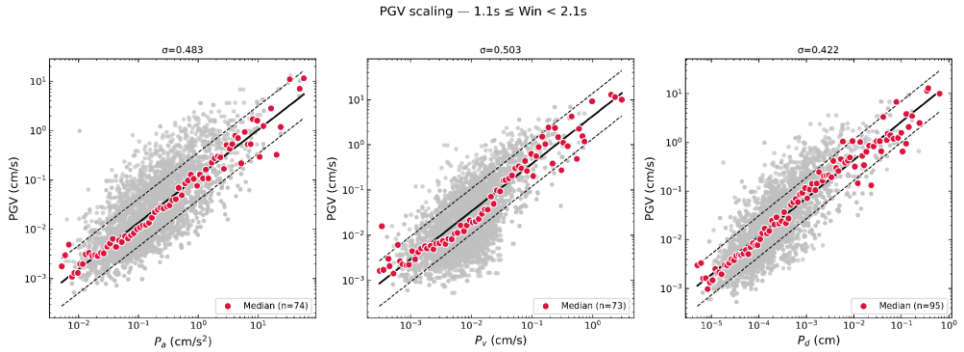

PGV scaling from Pa, Pv, and Pd — Win < 2.1 s

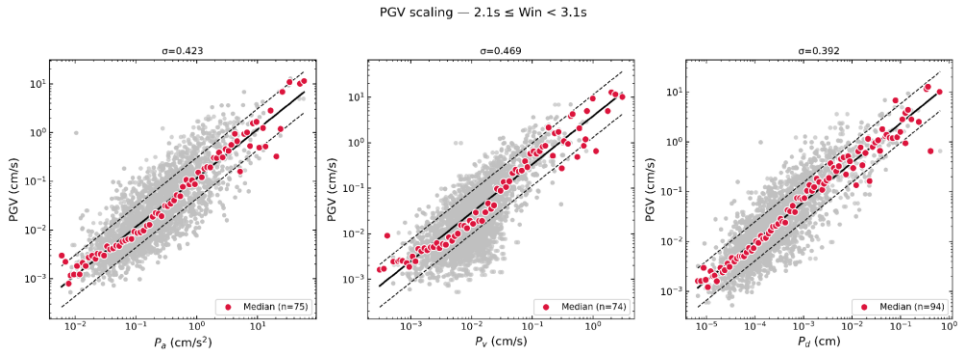

PGV scaling from Pa, Pv, and Pd — Win < 3.1 s

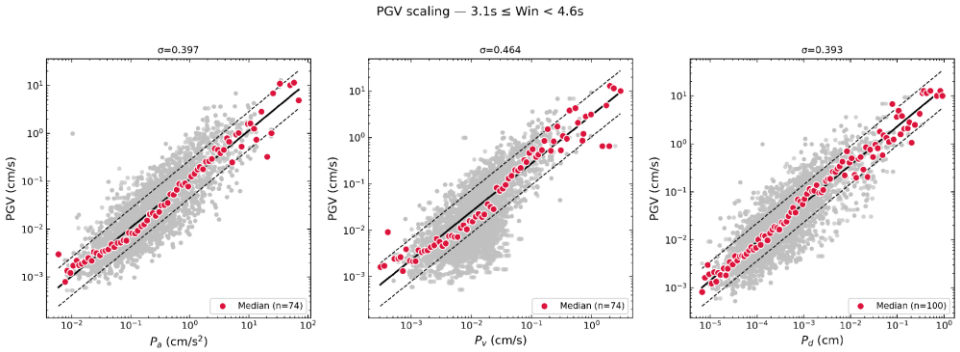

PGV scaling from Pa, Pv, and Pd — Win < 4.6 s

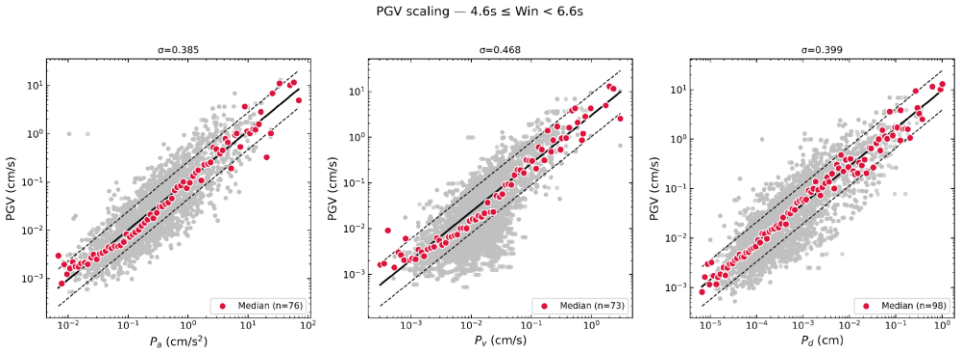

PGV scaling from Pa, Pv, and Pd — Win < 6.6 s

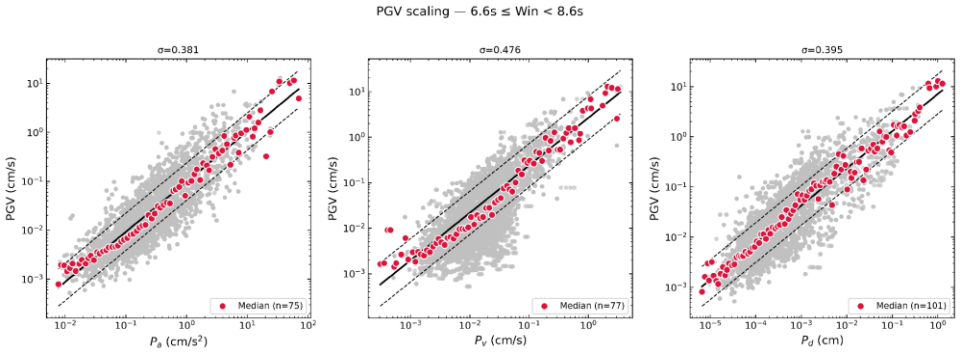

PGV scaling from Pa, Pv, and Pd — Win < 8.6 s

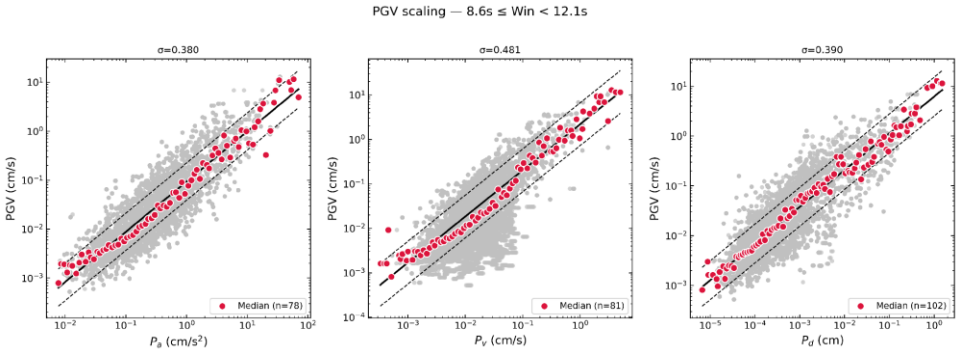

PGV scaling from Pa, Pv, and Pd — Win < 12.1 s

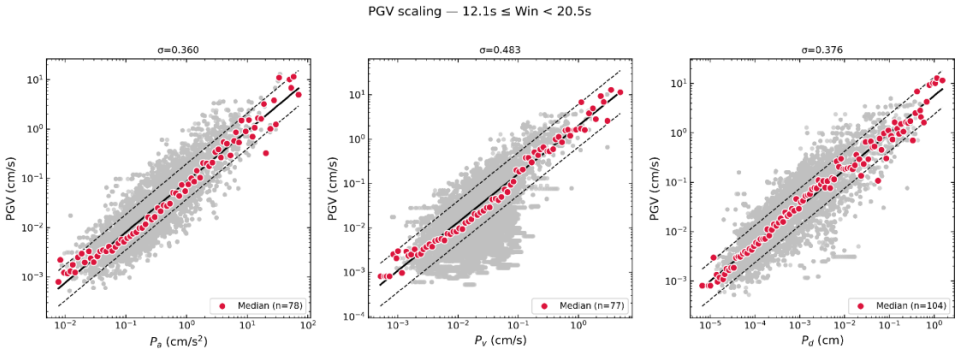

PGV scaling from Pa, Pv, and Pd — Win < 20 s

Appendix D: QuakeUp Playbacks

QuakeUp playback results for representative Marmara earthquakes are available online as supplementary material. The selected events span a magnitude range from Mw 3.4 to Mw 6.2 and include offshore Marmara earthquakes, inland events, and both moderate and damaging earthquakes.

Supplementary repository:
https://drive.google.com/drive/folders/1Qll1M5gAftBvj_UXBBkRXCahld4e-ZPC